Electrochemical ZrO_2 and Al_2O_3 coatings on SiC substrates

R. CHAIM, G. STARK AND L. GAL-OR
Department of Materials Engineering, Israel Institute of Metals Technion- Israel Institute of Technology Haifa, 32000 Israel

H. BESTGEN
Hoechst AG, Keramik Forschung, Frankfurt 80, Germany

SiC was electrochemically coated with ZrO_2 and with Al_2O_3 from 0.1 M aqueous solutions of metal–nitrate–hydrates with ethanol added. Amorphous zirconia and alumina coatings were formed with current densities from 10 to 70 mA cm^{-2}, and deposition durations of 1–60 min. The as-deposited coatings contained microcracks caused by drying shrinkage. Sintering of zirconia at 900 °C for 1 h and of alumina at 1200 °C for 2 h in air was accompanied by crystallization to a mixture of tetragonal and monoclinic phases in the former and to α-alumina in the latter. The absence of intermediate phases between the coatings and the substrates and the good adherence of the sintered coatings indicate the high-temperature stability of these coatings.

1. Introduction

Ceramic coatings seem ideal for using as materials at high temperatures and in severely corrosive environments [1, 2]. Forming ceramic coatings using an electrochemical method is a relatively new technique and has been used for the deposition of oxide coatings such as CeO_2 [3] and ZrO_2 [4, 5] and oxide/hydroxide of transition metals [6, 7] on to semiconducting and metallic substrates. However, no attempt has been made to apply similar coatings on to non-oxide substrates, although the latter are subject to high-temperature corrosion. The application of non-native oxide coatings on to non-oxide ceramic substrates could have significant implications on the high-temperature oxidation and stability of these materials. In this regard, zirconia has been found to lower the oxidation rate of SiC [8].

To form solid protective oxide coatings on non-oxide ceramics, several physical, chemical, and mechanical properties of the substrate and the coating material should first be considered. Among the properties needed by the substrate and coating material are high electrical conductivity and high melting point. The thermal expansion coefficients and the elastic moduli of both materials should be close to avoid mechanical failure of the coating. Although chemical interactions between the substrate and the coating are of great importance, their nature depends upon the specific substrate/coating system and the thermodynamic conditions during both fabrication and application. The affinity of the substrate and the coating for mutual chemical reactions during the processing should be borne in mind.

The present work describes the electrochemical formation of ZrO_2 and Al_2O_3 coatings on SiC substrates. The electrochemical deposition parameters and the microstructural evolution in the as-deposited and sintered coatings were characterized.

2. Experimental procedure

SiC (reaction bonded, ESK, Germany) bars of $3 \times 3 \times 50$ mm^3, having an electrical resistivity of 7 ohm cm, were used as the substrates. The bars were polished with 600 grit SiC abrasive paper and chemically etched for 15 min at 100 °C, in a solution of 10 g NaOH + 10 g $K_3Fe(CN)_6$ + 100 ml distilled water. The etched bars were cleaned with acetone in an ultrasonic bath and dried in air.

The electrolytes used were 0.1 M aqueous solutions of zirconyl–nitrate–hydrate ($ZrO(NO_3)_2 \cdot 9H_2O$) and aluminum–nitrate–hydrate ($Al(NO_3)_3 \cdot 9H_2O$). The electrolytic deposition set-up was similar to that reported previously [4]. Preliminary coating experiments using solutions with additions of different volumes of ethanol as wetting agent, had shown that the solutions with 50 vol% ethanol yield the most homogeneous and continuous coatings. The ratio of 1 : 1 salt solution to ethanol was therefore used. The pH of the zirconyl nitrate and aluminum nitrate solutions, prior to coating, was determined as 2.1 and 2.8, respectively.

A stabilized power supply (Model LLS 7120, Lambda, Carmiel, Israel) was used. The cell voltage and current were measured with AVO (Ampere-Volt-Ohm)-meters. Polarization curves were determined with the aid of a potentiostat (Model 350A, Princeton Applied Research, Princeton, NJ). The coating experiments were made using current densities ranging from 10 to 70 mA cm^{-2}, for 1–60 min, the cell voltage, the pH, and the temperature of the solution being

monitored throughout. The electrolyte temperature was kept at around 10 °C, using a cooling bath with ice. All experiments were performed without stirring. An area of 3 cm² was coated.

Generally, coating layers of a few microns in thickness were formed. The as-deposited gel-like coatings were dried in air for 24 h at room temperature. The coating weight was determined by weighing the specimens before and after deposition, with an accuracy of ± 0.05 mg. The coating thickness was measured with an optical microscope calibrated in the direction perpendicular to the field of vision (accuracy: ± 2.5 μm). The green density of the as-deposited coatings was then calculated on the basis of the deposit weight and thickness.

Some of the specimens were subjected to sintering heat treatments. The zirconia coatings were sintered in air for 1 h at 900 °C, the alumina coatings for 2 h at 1200 °C. Short oxidation treatments were also carried out on some of the Al_2O_3/SiC specimens, for 4 h at 1400 °C in air.

The phase content of the deposits was determined by X-ray diffraction (XRD) on a diffractometer (Model APD-1820, Philips Scientific and Analytical Equipments, Eindhoven, Holland) operated at 40 kV and 40 mA, monochromatized Cuk_α radiation and scanning speed of 0.4 deg min⁻¹ being used.

The microstructure of the deposits prior to and following sintering was characterized with the aid of a scanning electron microscope (SEM) (Model JSM-840, JEOL Ltd, London, UK) operated at 20 kV. The SEM specimens were gold evaporated.

3. Results
3.1. Electrochemical aspects
3.1.1. Polarization curves
Cathodic polarization curves were constructed with the SiC substrates (cathodes) versus a saturated calomel electrode (SCE) in solutions of 0.1 M $ZrO(NO_3)_2 \cdot 9H_2O$ + 50 vol% ethanol and in 0.1 M $Al(NO_3)_3 \cdot 9H_2O$ + 50 vol% ethanol. The electrode results are shown in Fig. 1. Generally, the polarization curves of the two solutions differ with respect to the magnitude of their limiting currents for a given potential. The polarization curves obtained represent at least two, and possibly three, of the conceivable cathodic reactions (see Section 4). However, these cannot be discerned, probably owing to the ohmic polarization caused by the non-conducting deposit which forms during the measurement.

3.1.2. The zirconia/SiC system
The coating weight versus current density plot for a duration of deposition of 6 min is shown in Fig. 2. The duration is limited by the cell voltage attained at high current densities, which must not exceed the maximum permissible output voltage of the power supply. A continuous increase in coating weight with current density was observed.

Electrochemical coatings obtained after periods longer than 6 min (namely 15, 30 and 60 min) resulted
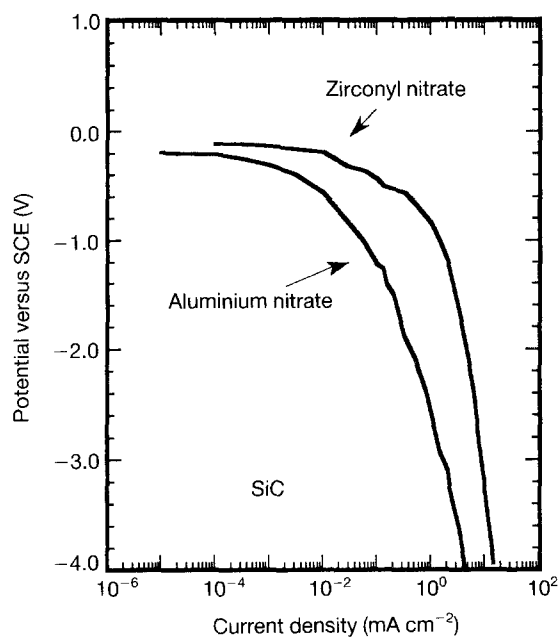

Figure 1 Cathodic polarization curves for SiC in 0.1 M solutions at 2 mV s⁻¹ scan.
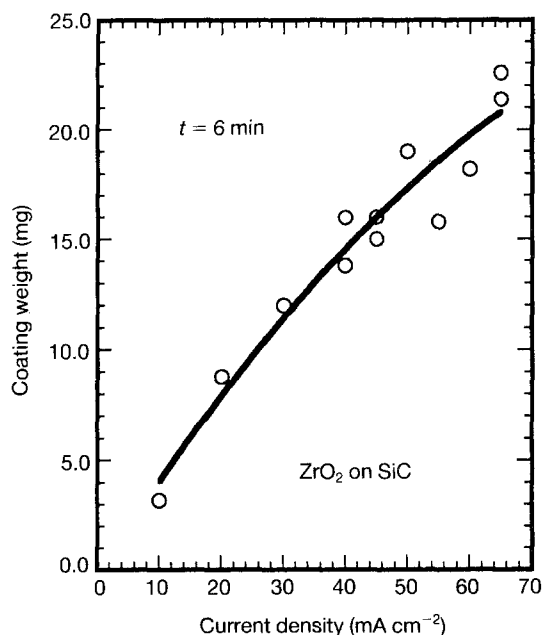

Figure 2 Zirconia coating weight showing a continuous increase with current density.

in low-quality coatings in the form of isolated coating "patches". In addition, significant sedimentation in the electrolytic bath was observed. After these long deposition times, enhanced evolution of gas bubbles (most probably molecular hydrogen) emerging from the cathode surfaces was observed. Visual inspection of the process confirmed that this effect led to spalling and sedimentation of the coating materials during the deposition process. After long deposition times, no correlation was observed between the coating weight and current density or deposition duration (see Table I). The coating experiments were therefore limited to shorter deposition times of the order of a few minutes. Nevertheless, at relatively low current densities, the increase in the cell voltage with coating build-up was moderate and permitted tracking of the deposition

TABLE I Zirconia coatings on SiC after long coating durations

Current density (mA cm^{-2})	Coating duration (min)	Coating weight (mg)
25	30	1.3
50	15	2.1
50	30	1.35
50	60	1.3
75	30	0.5
100	30	1.4
100	60	1.0

process for longer durations. The coating weight versus deposition duration at a current density of 20 mA cm^{-2} is shown in Fig. 3. A continuous increase in the coating weight with time was recorded.
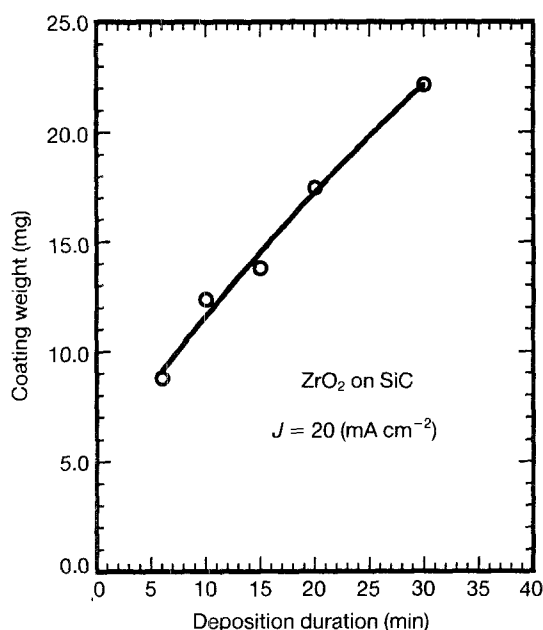

Figure 3 Coating weight versus duration of deposition showing a continuous increase at low current densities.
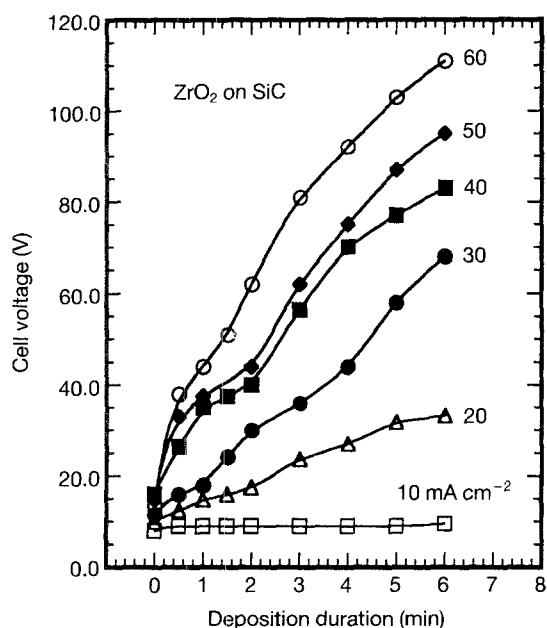
The cell voltage always increased with deposition time, as shown in Fig. 4. Generally, the higher the current densities, the steeper were the slopes observed. The voltage increase was almost linear at the lower current densities, but at the higher current densities, the cell voltage increased rapidly at the beginning of the deposition, and more modestly as deposition proceeded. This effect is related to the formation and thickening of the low-conducting deposits on the cathode surfaces which, in turn, increases the potential drop across the deposit. At a given deposition duration, the increase in current density is expected to accelerate the rate of deposition, hence the increase in the potential drop across the deposit.

The pH of the zirconyl electrolyte solution was found to increase to up to 4 after a relatively short time (12–15 s) from the beginning of the deposition process. Generally, the pH reached a maximum, which was followed by a reduction to the saturation value after longer durations (beyond 2 min). The pH maxima as well as the saturation values increased with the current density. The actual pH values, near the cathode, are expected to be higher, since the values measured were taken in the bulk of the solution.

The relative green densities of the deposits were calculated on the basis of their net weights and thicknesses, a 23 vol % of microcracks in the as-dried coatings being taken into account. (The latter was determined using optical microscope images; the thickness was averaged over five measurements made at different locations of the coating and based on the theoretical density of 6.0 g cm^{-3} for zirconia). These results are shown in Fig. 5 as a function of current density and indicate higher green densities in the deposits being formed at lower current densities.

3.1.3. The alumina/SiC system

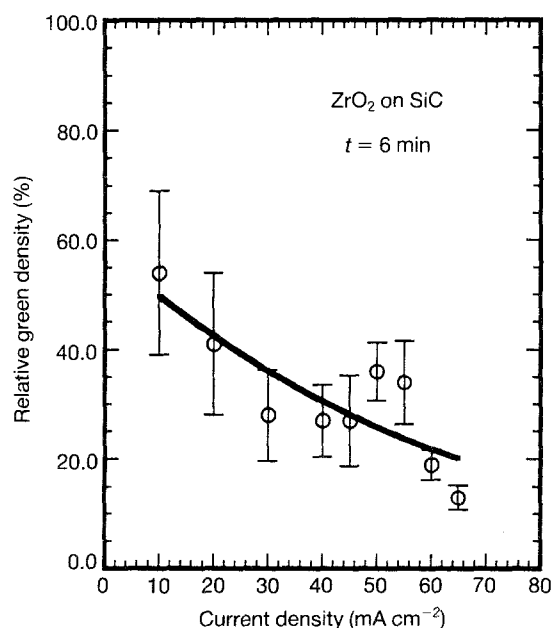Alumina deposits exhibited poor adherence to the SiC substrates and were sedimented at the bottom of the

Figure 4 Variation of the cell voltage with duration of deposition at different current densities.

Figure 5 Relative green density of the zirconia coatings versus current density.
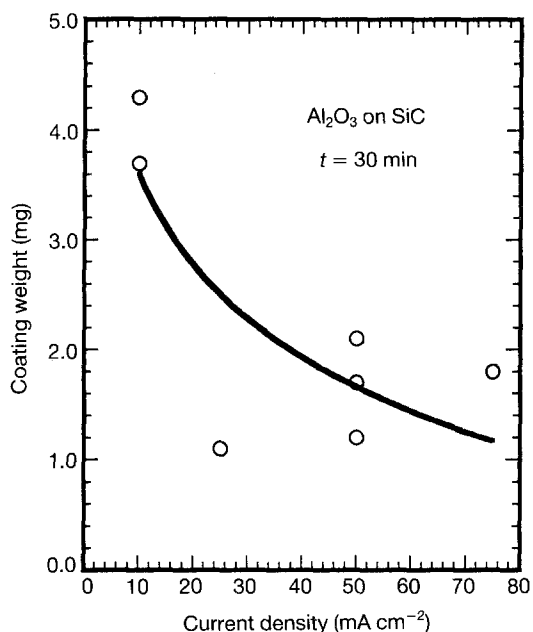
6243

Figure 6 Alumina coating weight, showing a rapid reduction with current density, at long deposition durations.
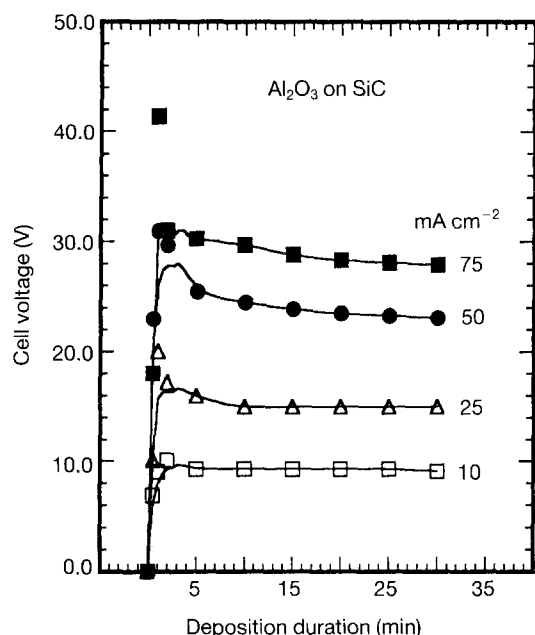

Figure 7 Variation of the cell voltage with duration of deposition at different current densities for alumina deposits.

electrolytic bath. After a deposition period of 30 min, a continuous reduction in coating weight was observed with increasing current density (Fig. 6). Deposit spallation from the cathode was due to the formation of gas bubbles, especially at high current densities, similar to that observed in the zirconia/SiC system. However, in the present system, the cell voltage increased rapidly to a peak value within two minutes or less from the start of deposition (Fig. 7). The peak was followed by a drop to a saturation value. The level of the peak as well as the saturation voltage increased with current density, as did the time at which the peak value was reached. The time pattern of the pH was similar to that found in the ZrO_2/SiC system.

3.2. Microstructural aspects

SEM images of the SiC substrates before (Fig. 8a) and after chemical etching (Fig. 8b), showed a significant roughening of the surface due to the etching. This was probably caused by preferential etching of the residual silicon (see Fig. 11) present at the SiC grain-boundaries.

The wet and continuous as-deposited coatings had a gel-like transparent appearance, regardless of the coating material. However, dry zirconia coatings remained colourless and transparent, while those of alumina became white and opaque. The coating thickness varied within the range of 1–10 μm. The dry coatings of both oxides often contained microcracks and thus exhibited the "cracked-mud" morphology (Figs 9a and 10a). This type of microcracking was observed especially in regions of thick coating and was related to drying shrinkage. Nevertheless, regions with thin coatings were smooth and almost crack-free (Figs 9b and 10b). X-ray diffraction spectra from the as-deposited zirconia (Fig. 11a) and alumina coatings (Fig. 12a) showed reflections of SiC (mainly of the 6H polytype) and residual Si only, indicating the amorphous nature of both deposits.

Sintering heat treatment of the zirconia coatings on SiC for 1 h at 900 °C caused crystallization of the amorphous zirconia into a mixture of tetragonal and monoclinic phases, as shown in Fig. 11b. Similarly, a heat treatment of the alumina coatings on SiC for 2 h at 1200 °C, caused the amorphous alumina to crystallize to α-Al_2O_3 (corundum) (Fig. 12b). In addition, in
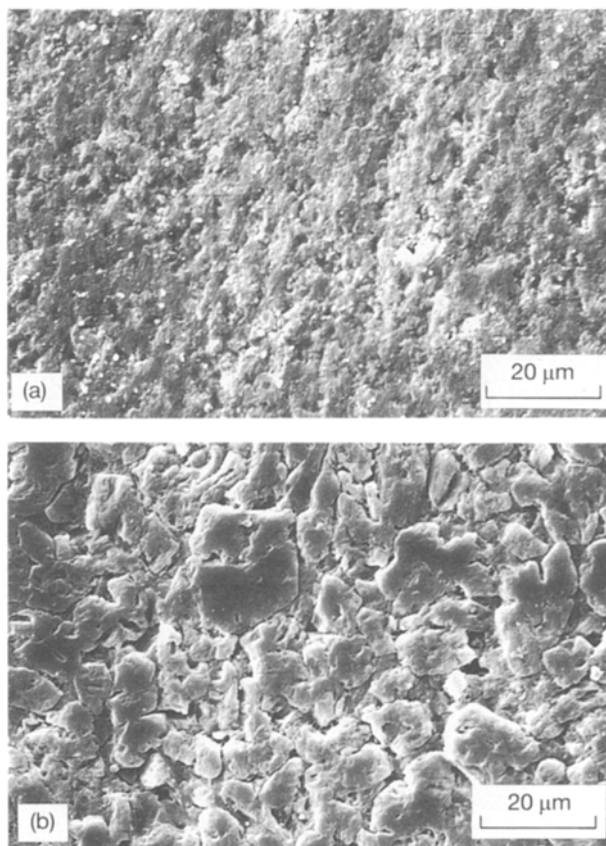

Figure 8 SEM images of the: (a) as-received; and (b) chemically etch SiC substrates showing surface roughening owing to the etching.
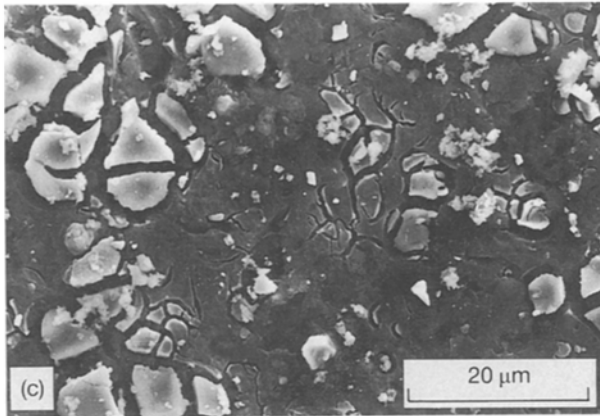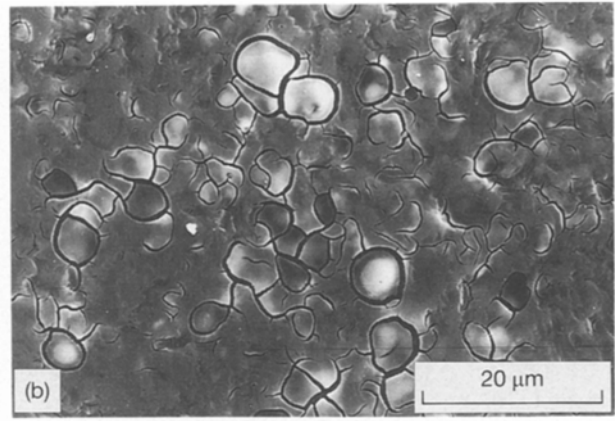
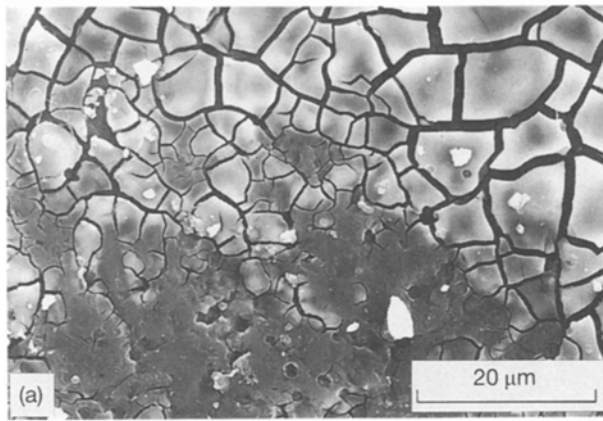the Al_2O_3/SiC system, some weak reflections of tridymite (SiO_2) were also identified, which most probably arise due to oxidation of the SiC substrate when

exposed to air by microcracks. In both types of oxide coatings the sintering shrinkage resulted in a widening of the microcrack gaps between the coating islands, regardless of the coating thickness (Fig. 9c and d and Fig. 10c and d).

Preliminary short-term oxidation experiments in air for 4 h at 1400 °C showed the Al_2O_3 coating to be stable and adherent to the SiC substrate (Fig. 13a and b). However, under the same oxidation conditions, the uncoated SiC surfaces underwent significant thermal etching (Fig. 13c). The exposed grain structure in the latter may also be due to active oxidation of the SiC.
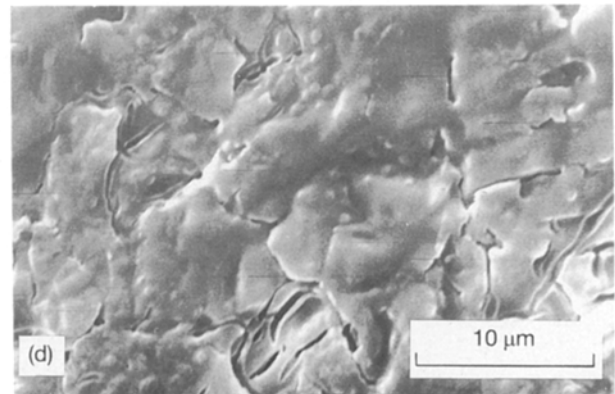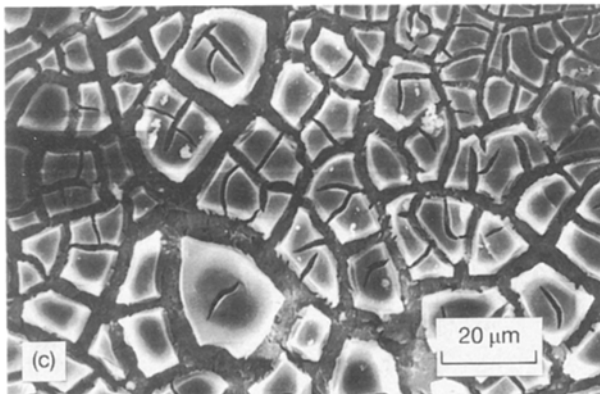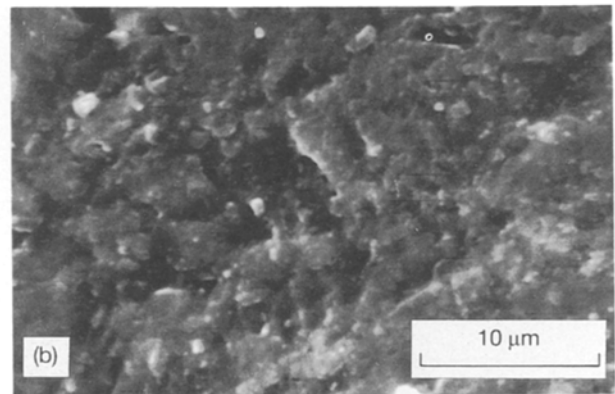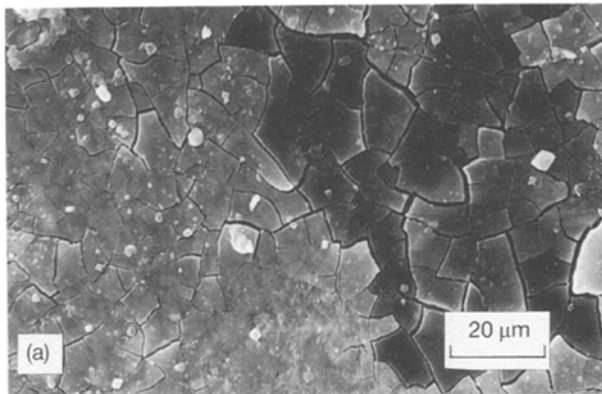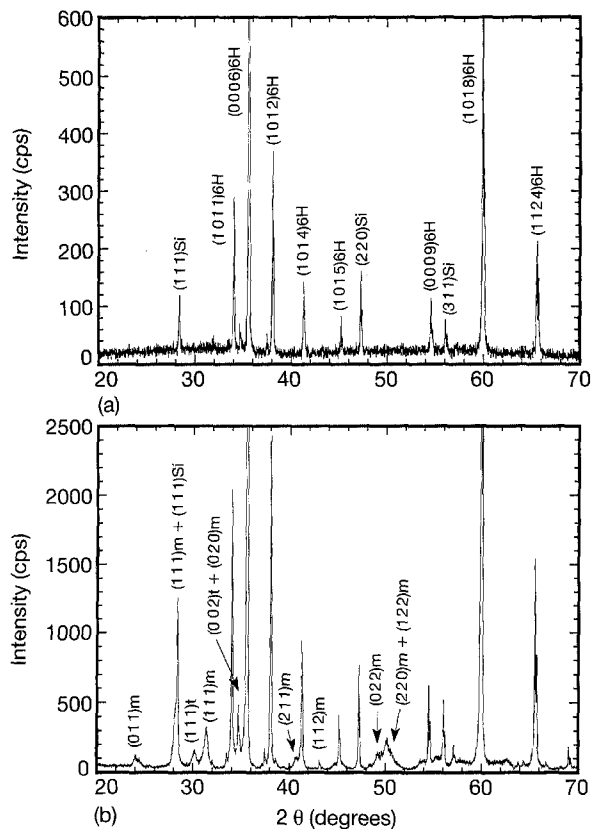
Figure 11 X-ray diffraction spectra of: (a) as-deposited; and (b) as-sintered zirconia on an SiC substrate. The as-deposited coatings were amorphous but crystallized during sintering into a mixture of tetragonal and monoclinic polymorphs. 6H. (SiC hexagonal polymorph; Si: silicon; M: monoclinic zirconia; t: tetragonal zirconia).
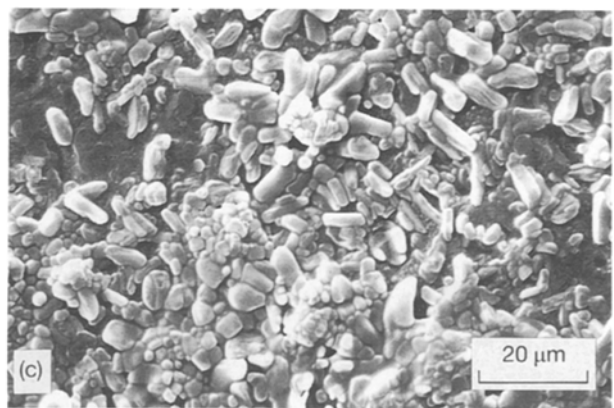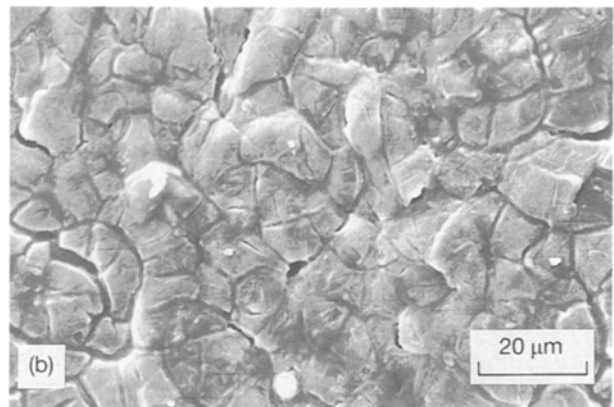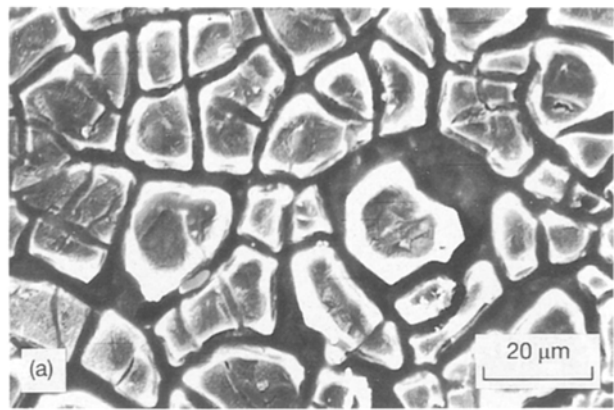

Figure 12 X-ray diffraction spectra of: (a) as-deposited; and (b) as-sintered alumina on SiC. The as-deposited coatings were amorphous but crystallized during sintering to α-alumina (corundum). (15 R and 2H: SiC rhombohedral and hexagonal polymorphs, respectively; alpha: hexagonal alumina).

Figure 13 SEM images of sintered alumina coatings on SiC at the: (a) thick; and (b) thin coating regions, subjected to oxidation treatment for 4 h at 1400 °C within a graphite crucible. Both regions exhibit structural stability and good adherence to the SiC substrate. (c) Uncoated region showing strong active oxidation in the similar oxidation conditions.

4. Discussion

Electrochemical synthesis of zirconia may be described by several consecutive reactions which include [4]:

i) Dissociation of the zirconyl nitrate:

$$ZrO(NO_3)_2 \rightarrow ZrO^{2+} + 2NO_3^-$$
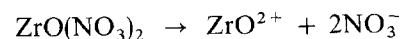
ii) Hydrolysis of the zirconyl ions:

$$ZrO^{2+} + H_2O \rightarrow Zr(OH)_2^{2+}$$

iii) Reaction with the hydroxyl groups, generated at the cathode, to form zirconium hydroxide which is deposited on the cathode:

$$Zr(OH)_2^{2+} + 2(OH)^- \rightarrow Zr(OH)_4$$

iv) Dehydration during drying, to form amorphous zirconia:

$$Zr(OH)_4 \rightarrow ZrO_2 + 2H_2O$$

The reactions appropriate to the case of alumina deposition may be described as follows:

i) Dissociation of the aluminum nitrate:

$$Al(NO_3)_3 \rightarrow Al^{3+} + 3NO_3^-$$

ii) Formation of hydroxide:

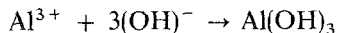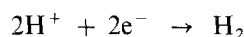$$Al^{3+} + 3(OH)^- \rightarrow Al(OH)_3$$

iii) Dehydration during drying to form amorphous alumina:

$$2Al(OH)_3 \rightarrow Al_2O_3 + 3H_2O$$

The hydroxyls needed for the formation of the hydroxide are produced by reduction reactions involving the dissolved oxygen, nitrate ions, and water.

In addition, hydrogen is formed at the cathode and evolves as a molecular gas according to the following reaction:

$$2H^+ + 2e^- \rightarrow H_2$$

The coating build-up can be described as the formation of cationic species, such as $[Zr(OH)(OH_2)_7]^{3+}$ and $[Al(OH)(OH_2)_5]^{2+}$ in the acidic aqueous solutions [9, 10]. Relevant calculations by Zhang and Glasser [11] using the partial charge model [9] have shown that stable oxy-hydroxide or hydroxide species can be obtained for most Al(3 +) and Zr(4 +) precursors. Finally, these oxy-hydroxide species coagulate and migrate by electrophoresis towards the cathode. The rate of the coating build-up depends on the flux of the species towards the cathode. Thus, an increase in the current density accelerates the deposition rate.

The transparent and colourless nature of the dry zirconia coatings indicates a gel-like open network of its polymerized oxy-hydroxide, whereas the white colour and the translucent nature of the alumina coatings may indicate the formation of coarser and possibly water-free particles. Similar changes in the transparency of the zirconia gel were found to be due to the change in the solvent water ratio [12].

The amorphous nature of the zirconia and the alumina coatings in the present work contrasts with the crystalline nature of chromia coatings, studied in a previous work [13]. (It should be noted that chromia and alumina have a similar corundum-type crystal structure). The difference in the crystallinity of these oxides may be related to different factors, such as the covalent character of the M–O bonds and the charge transfer regime at the cathode. Considering the z/d ratios, where d is the M–O interatomic distance (the ionic radius of M^{z+} plus 0.138 nm as given by Shannon and Prewitt [14]), appropriate values of 0.140, 0.157 and 0.178 nm may be calculated for Cr_2O_3, Al_2O_3 and ZrO_2, respectively. According to Mesmer and Baes [10], the higher the z/d ratio, the higher the covalent character of the M–O bond; hence the increase in the tendency of the oxide to form an amorphous structure. This trend is in agreement with the

amorphous nature of the alumina and zirconia coatings.

Although no data are available on the electrical conductivities of the aluminum and the chromium hydroxides, a significant difference (of the order of $\approx 10^7$ ohm cm) exists between the electrical conductivities of their respective oxides [15]. Actually, while alumina is considered to be a very good insulator, chromia exhibits a semiconducting behaviour. Zirconia also behaves as an insulator. Thus, a higher mobility of the charge and its homogeneous distribution on the cathode surfaces may also be responsible for the enhanced trends in the crystallization and growth of the Cr_2O_3 crystals, compared with the amorphous nature of the Al_2O_3 and ZrO_2 oxides.

Formation of amorphous zirconia and alumina through chemical precipitation of their hydroxides is well documented in the literature [16–21]. Although ZrO_2 and Al_2O_3 are not the classic glass-former oxides, they are considered to be conditional glass-formers [22]. The co-ordination number of Al and O ions in Al_2O_3 is 6:3, thus oxygen does not form Al–O–Al bridges. Nevertheless, the structure is based on the closest packing of the oxygen ions. Since the Al–O bond has a 61 % ionic and 39 % covalent character (63 % and 37 % respectively in ZrO_2) the bond is expected to have some flexibility. This structural flexibility could be a major factor in the formation of amorphous Al_2O_3 as well as in other ionic oxides that are based on the nearly closest packing of the oxygen ions.

In addition, special attention should be given to the presence of hydrogen in the deposits. Hydrogen in the oxide coating can lead to increased structural flexibility by forming M–H or M–OH bonds in addition to the normal M–O bonds. If the corresponding metal oxy-hydroxide has various polymorphs (as have Al_2O_3 and ZrO_2), then various conformations of the M–OH bond may exist and in turn increase the tendency toward amorphism.

Concerning the cracked morphology of the present coatings, the anisotropic drying shrinkages (which are typical of green ceramic coatings) are considered to have a major effect on the crack pattern. Pertinent calculations by Thouless [23] and Hu et al. [24] show that cracking may take place in thin coating films over elastic substrates (e.g. ceramics), when the coating thickness exceeds a critical value. (This value is proportional to the square of the fracture toughness/residual stress ratio). The crack-free nature of the thin coating regions is in agreement with this model and confirms that the residual stresses due to drying are responsible for the microcracking. In addition, a roughening of the SiC substrate surface by chemical etching may cause serious stress concentrations within the coatings [25], thus enhancing the microcracking. Nevertheless, surface roughening improves the physical bonding between the coating and the substrate. Certainly, controlled drying is necessary to obtain continuous crack-free coatings.

Switzer [5] found that the pH increase in the electrochemical deposition of zirconia leads to an increase in the surface area of the resulting powder (i.e. finer

particle size). Similar pH effects were reported in the synthesis of zirconia powders by chemical precipitation [16, 17] and in the hydrothermal treatment of zirconia salt solutions [18–20]. Thus, the increase in pH that was associated with an increase in the current density, may also result in finer complex precipitates in the electrolyte. Consequently, electrophoresis of finer species is expected to build green coatings with higher porosity, in agreement with the present results (Fig. 5). The accelerated build-up of the deposits at high current densities is also expected to yield a more porous deposit.

The microstructural evolution and the phase content of the sintered deposits indicate the high-temperature stability of these oxide coatings, which crystallized to their stable polymorphs (i.e. α–Al_2O_3 and monoclinic ZrO_2, respectively). The presence of silica in the Al_2O_3/SiC system arises from the oxidation of SiC under microcracks. However, the absence of mullite and zircon in the Al_2O_3/SiC and ZrO_2/SiC systems, respectively, along with the good adherence of the coatings to the substrate after sintering and oxidation, demonstrate the chemical and physical high-temperature stability of these coatings.

Acknowledgements

References

1. G. FISHER, Am. Ceram. Soc. Bull. **65** (1986) 283.
2. T. E. SCHMID and R. J. HECHT, Ceram. Eng. Sci. Proc. **9** (1988) 1089.
3. J. A. SWITZER, Bull. Am. Ceram. Soc. **66** (1987) 1521.
4. L. GAL-OR, I. SILBERMAN and R. CHAIM, J. Electrochem. Soc. **138** (1991) 1939.
5. J. A. SWITZER and R. J. PHILIPS, in "Better Ceramics Through Chemistry III," Mat. Res. Soc. Symp. Proc., Vol. 121, edited by C. J. Brinker, D. E. Clarck, and D. R. Ulrich, MRS, Pittsburgh (1988) pp. 111–14.
6. D. TENCH and L. F. WARREN, J. Electrochem. Soc. **130** (1983) 869.
7. K.-C. HO, J. Electrochem. Soc. **134** (1987) 52C.
8. W. LUECKE, D. L. KOHLSTEDT and S. B. DAWES, J. Mater. Sci. **25** (1990) 5118.
9. J. LIVAGE and M. HENRY, in "Ultrastructure Processing of Advanced Ceramics", edited by J. D. Mackenzie and D. R. Ulrich, John Wiley & Sons, NY (1988) pp. 183–95.
10. R. E. MESMER and C. F. BAES, Jr., in "Better Ceramics Through Chemistry IV", Mat. Res. Soc. Symp. Proc. Vol. 180, edited by B. J. J. Zelinski, C. J. Brinker, D. E. Clark, and D. R. Ulrich, MRS, Pittsburgh (1991) pp. 85–96.
11. W. ZHANG and F. P. GLASSER, J. Mater. Sci. **28** (1993) 1129.
12. D. KUNDU and D. GANGULI, J. Mater. Sci. Lett. **5** (1986) 293.
13. R. CHAIM, S. ALMALEH-ROCKMAN, L. GAL-OR and H. BESTGEN, J. Am. Ceram. Soc., to be published.
14. R. D. SHANNON and C. T. PREWITT, Acta Cryst. B25 (1969) 925.
15. E. ELSHEREEFY and M. F. R. FOUDA, J. Mater. Sci. Lett. **10** (1991) 299.
16. A. BLEIER and R. M. CANNON, in "Better Ceramics Through Chemistry II", edited by C. J. Brinker, D. E. Clark and D. R. Ulrich, vol. 73, MRS, Pittsburgh (1987) pp. 71–78.
17. R. P. DENKEWICZ, Jr., K. S. TENHUISEN, and J. H. ADAIR, J. Mater. Res. **5** (1990) 2698.
18. R. SRINIVASAN, R. De ANGELIS and B. H. DAVIS, J. Mater. Res. **1** (1986) 583.
19. G. T. MAMOTT, P. BARNES, S. E. TARLING, S. L. JONES and C. J. NORMAN, J. Mater. Sci. **26** (1991) 4054.
20. X. TURRILLAS, P. BARNES, D. HAUSERMANN, S. L. JONES and C. J. NORMAN, J. Mater. Res. **8** (1993) 163.
21. J. D. MACKENZIE, in "Ultrastructure Processing of Advanced Ceramics", edited by J. D. Mackenzie and D. R. Ulrich, John Wiley & Sons, NY (1988) pp. 589–601.
22. H. RAWSON, in "Inorganic Glass-forming Systems", Academic Press, London (1967) p. 9.
23. M. D. THOULESS, J. Am. Ceram. Soc. **73** (1990) 2144.
24. M. S. HU, M. D. THOULESS and A. G. EVANS, Acta Metall. **36** (1988) 1301.
25. R. L. MULLEN, R. C. HENDRICKS and G. McDONALD, Ceram. Eng. Sci. Proc. **8** (1987) 559.